Adaptive Grid Refinement for Two-Dimensional and Three-Dimensional Nonhydrostatic Atmospheric Flow

WILLIAM C. SKAMAROCK AND JOSEPH B. KLEMP

National Center for Atmospheric Research, Boulder, Colorado*

(Manuscript received 7 February 1992, in final form 19 July 1992)

ABSTRACT

Although atmospheric phenomena tend to be localized in both time and space, numerical models generally employ only uniform discretizations or fixed nested grids. An adaptive grid technique implemented in 2D and 3D nonhydrostatic elastic atmospheric models is described. The adaptive technique makes use of separate rectangular refinements to increase resolution where truncation error estimates are large. Multiple, rotated, overlapping grids are used along with an arbitrary number of discrete grid-refinement levels. Refinements are placed and removed automatically during the integration based on estimates of the truncation error in the evolving solution. The technique can be viewed as an extension of the nesting technique often used in atmospheric models.

The adaptive model integrates the compressible, nonhydrostatic equations of motion. Although sound waves are not significant in the solution, they do constrain the time step. A splitting technique is used to accommodate the sound waves by advancing certain terms with a separate smaller time step. The terms responsible for gravity waves are also integrated with the smaller time step, and with the acoustic modes filtered through the use of divergence damping, the resulting model can be run as efficiently as hydrostatic models. Boundary conditions developed for the splitting technique in the adaptive framework are described and tested in the 2D and 3D models. The adaptive technique is shown to be efficient when compared to single fixed-grid simulations. Two new features are included in the basic solver.

Also considered are additional complications that arise because of the necessary use of parameterized physics. The dependence of many parameterizations on grid scale creates difficulties in evaluating truncation error and raises more general questions concerning solution error in nested and adaptive models.

1. Introduction

The increasing speed and memory of supercomputers allows for the explicit resolution of an ever larger range of scales of atmospheric motion in a single computation. This can be seen clearly in the global forecast models that are now being run regularly with spatial resolution of order 100 km. Atmospheric motions of interest, though, span many more scales than it is possible to capture explicitly in a single computation. Nonhydrostatic motions may contain significant features on scales ranging from several meters to tens of kilometers with time scales of seconds to many hours. Hydrostatic motions, in which nonhydrostatic features are embedded, have scales orders of magnitude larger than the nonhydrostatic motions. The inability to explicitly resolve this large range of motion scales in numerical models has hindered the study of scale-interaction issues.

We believe that the next generation of mesoscale–cloud-scale models should be suitable for studying scale interactions between nonhydrostatic and hydrostatic motions and would benefit from the utilization of adaptive grid-refinement techniques. The purpose of this paper is to present an approach for selectively enhancing resolution within portions of a nonhydrostatic mesoscale model through the use of adaptive grids. The adaptive method was developed by Berger and Oliger (1984) and uses multiple overlapping fine grids to increase resolution. The fine grids function similarly to the more conventional two-way interactive nested grids. However, the adaptive grids can change size, shape, location, and number in response to evolving structure in the simulation. In the next section, we will briefly review nested and adaptive modeling techniques and describe the Berger and Oliger adaptive method. In section 3, we present the equations and discretization used in a simple 2D model. We employ an elastic equation set and a variant of the solution technique described in Klemp and Wilhelmson (1978), which includes a sound-wave filter and a modified split-time-step solution method. Two-dimensional adaptive simulations of a gravity current are shown in section 4. Timing results demonstrate that the adaptive method is effective. The gravity-current simulations also illus-

* The National Center for Atmospheric Research is sponsored by the National Science Foundation.

Corresponding author address: William C. Skamarock, National Center for Atmospheric Research, P.O. Box 3000, Boulder, CO 80307-3000.

trate the consequences of using parameterizations that depend on the grid scale. These parameterizations are responsible for nonconvergence of the solutions and make model verification difficult. In section 5, results from a 3D, fully compressible, nonhydrostatic, moist interactive–adaptive cloud model demonstrate the robustness of the numerical algorithms and the straightforward extension of most 2D adaptive algorithms to the moist 3D problem.

2. Nested and adaptive modeling techniques

For the 2D and 3D models we employ the adaptive mesh refinement technique (AMR) of Berger and Oliger (1984) and use the nonhydrostatic, compressible equations of motion. This section begins with an outline of the AMR procedure, continues with a brief review of other adaptive solution approaches, and concludes with a discussion of other nested-grid models used for atmospheric simulations. AMR has much in common with the nested-grid models and various grid nesting issues will be considered.

a. Adaptive mesh refinement

AMR is one in a class of techniques for automatically improving the solution accuracy in the numerical integration of a set of partial differential equations. AMR is a *local* refinement technique in that it adds grid points as a means of improving the solution accuracy, as opposed to a *global* refinement technique, which redistributes grid points. AMR has been successfully used for many fluid-flow problems, including large-scale hydrostatic atmospheric flows (Skamarock et al. 1989), transonic airflow (Berger and Jameson 1985; Berger and Colella 1989), and steady-state and time-dependent Navier–Stokes equations (Caruso et al. 1986; Perng 1990).

The adaptive solution procedure for hyperbolic systems begins with a coarse-grid solution valid at some time t. The numerical error (normally the truncation error) in the solution is estimated at the grid points. Where the error is greater than some predetermined tolerance, the points are flagged, indicating that the area needs refinement. Rectangles (the fine grids) are fit enclosing these points. The grids may overlap and they need not be aligned with the base grid. Initial conditions for the fine grids are interpolated from the coarse grid or possibly from previously existing fine grids. Next, the coarse and fine grids are integrated from time t to time $t + \Delta t$ (coarse). The time steps on the fine grids are smaller than those on the coarse grid in order to keep $\Delta x/\Delta t$ constant on the different grids (as is appropriate for hyperbolic systems). Fine-grid boundary values are interpolated, spatially and temporally, from the coarse grid or from the fine grids in places where fine grids overlap. When all grids have been integrated over the coarse time interval, the solution at the coarse grid points that lie inside of a fine grid are replaced (updated) with an appropriately averaged value from the fine grids. This process may now be repeated for the next time step. The error estimate and re-creation of the fine grids need not occur at each time step but rather only at specified intervals. By periodically reestimating the error and creating new fine grids, the grids can move with whatever is responsible for the high error, usually some prominent solution feature. A fully adaptive method is achieved by allowing for error estimation on the fine grids and the introduction of still finer grids.

The philosophy of AMR is to use regular finer grids to resolve features that are not resolved on the coarser grids and to do this automatically. Also, phenomena not resolved on the coarse grid are not allowed to propagate through a fine-grid boundary out onto the coarse grid; rather, the fine grids are replaced so that the refinement moves with the feature. If phenomena reorient, grow, or decay, then the fine grids are reoriented, changed in size, added, or removed. It is in this capacity that AMR differs from traditional nested models where grids are stationary or where a single fixed-size grid follows a single solution feature.

AMR offers certain advantages over other adaptive approaches. All grids are regular; hence, preexisting solvers can be used with the AMR routines as well as fast solvers that work only on regular grids. Grid regularity results in shortened development time and preserves and extends previous model development efforts. Also, the experience derived from constructing nested models can provide guidance in the development of more robust boundary condition and updating routines. Finally, the AMR routines can be used with parallel and distributed solution techniques.

This paper outlines boundary condition specification for the interior fine grids, updating procedures, and presents general test results for the nested–adaptive grid approach using a nonhydrostatic, elastic set of equations. Details of the error-estimate procedures are given in Skamarock (1989). Algorithmic details and data structures, along with a more general overview of AMR, can be found in Berger and Oliger (1984).

b. Other adaptive approaches

Several approaches have been developed for adaptive grid refinement. Other options that can be classified as local refinement methods involve adding grid points or dividing grid cells (see Dannenhoffer and Baron 1986; Kallinderis and Baron 1989) or dividing elements (Hawken et al. 1991). In these approaches, there is only one grid, and the irregularity of the grid gives rise to a complex solution algorithm and prevents the use of standard solvers. The primary advantage these techniques have over AMR is that the refinement can be more easily tailored to the phenomena and that fewer grid points need to be used. We know of no efforts to construct an atmospheric model using these approaches.

Global refinement methods are receiving increasing attention from atmospheric modelers. In the global refinement techniques, grid points move automatically so that they are clustered in regions where the solution error is high. The governing equations are transformed from physical space, where the grid is nonuniform, possibly nonorthogonal, and in motion, to computational space, where the grid is regular and stationary.

The global refinement techniques are not Lagrangian; the grid points are not advected by the flow. The distribution of points must be computed at each time and the most popular methods involve solving a set of elliptic equations that are derived from a combination of variational problems. The variational problems attempt to maintain certain grid properties, typically orthogonality and grid smoothness. A weighting function serves to attract points to regions where they are needed.

The global refinement techniques offer one major advantage over most local refinement techniques—the transition between regions of high resolution and low resolution is smooth. This feature removes some of the wave-reflection and wave-dispersion problems that can occur in local refinement methods where points are added to a regular grid or where nested fine grids are used. Although this feature is highly desirable, the global methods also have several undesirable features. First, the grid is no longer regular. The transformation to computational space produces numerous additional terms that need evaluation, and the transformation metrics also must be recomputed each time step. The grid must be generated anew each time step, most often by solving a set of elliptic equations. Also, in time-dependent problems where the equations are integrated with explicit methods, the time step is limited by the stable time step for the smallest grid volume. Finally, increasing the resolution in one region reduces resolution in another, and it is only by adding points that a given overall solution accuracy can be guaranteed (here we are concerned with the maximum local error). Even with these potential drawbacks, progress is being made in developing economic global refinement models for atmospheric computations (Dietachmayer and Droegemeier 1992; Dietachmayer 1992).

c. *Nested-grid models*

The fine grids in AMR function as two-way interactive nested grids commonly used in atmospheric models. Grid nesting has been used extensively in hydrostatic models. Examples in a research setting are the Pennsylvania State University–National Center for Atmospheric Research Mesoscale Model (MM4) (Zhang et al. 1986) and, in an operational setting, the NGM used at the National Meteorological Center (Hoke et al. 1989). In both cases, the grids are fixed in both number and location, though recently the MM4 has incorporated the ability to have multiple fine grids that move in time (G. Grell, personal communication). Applications where the fine grids are allowed to move include the hurricane models of Harrison (1973) and Jones (1977). These nested models are not truly adaptive in that it must be known a priori where increased resolution will be needed.

There are fewer nested nonhydrostatic models. Clark and Farley (1984) constructed a nested model based on an anelastic set of equations. The system allows multiple nesting, but they cannot be rotated with respect to the base grid, and multiple, overlapping grids cannot be used on the same refinement level. Solution of the elliptic pressure equation in the nested configuration does not appear to impose any significant computational penalty. Chen (1991) describes a nested nonhydrostatic model that uses a compressible (elastic) equation set. This nested model does not require the solution of any multidimensional elliptic equation.

We have chosen to use the compressible nonhydrostatic equations as opposed to the anelastic set for several reasons. While the computational cost of integrating either set on a single grid or in a simply nested system is comparable, integrating the anelastic set on multiple overlapping grids is very expensive compared with the elastic set. The solution of the pressure equation on overlapping grids must be treated as a set of coupled problems. Solution techniques exist (See Caruso et al. 1986; Oliger et al. 1990; Thompson and Ferziger 1989), but all these require some form of iteration among the overlapping grids. Solution of the elastic set on overlapping grids requires no information exchange between grids when integrating over a time step.

The use of overlapping, arbitrarily oriented fine grids is highly desirable when trying to refine features that are not aligned with the base grid. In particular, fine grids can be aligned with the flows, thus reducing truncation error, and fewer overall grid points need be used in the refinements. An example of this is given in Fig. 1.

Fine-grid rotation is difficult to achieve when using the anelastic system or any system in which exact mass conservation is important, because interpolations for boundary conditions and averaging for updating must be conservative. Conservation of mass or any other quantity in the nested system has been considered by Clark and Farley (1984), Kurihara et al. (1979), and others, and it can be stated as follows. Given the quantity Φ on the coarse grid and the corresponding quantity ϕ on the nested fine grid, where Φ and ϕ are fluxes, the quantities will be conserved in the interpolation and averaging procedures if

$$\sum \phi_i \Delta l = \Phi_I \Delta L, \tag{1}$$

where Δl is the grid length on the fine grid, ΔL is the grid length on the coarse grid, and the fine-grid variable is summed over a single coarse-grid interval. It is also required that the fine grid and coarse grid are aligned,

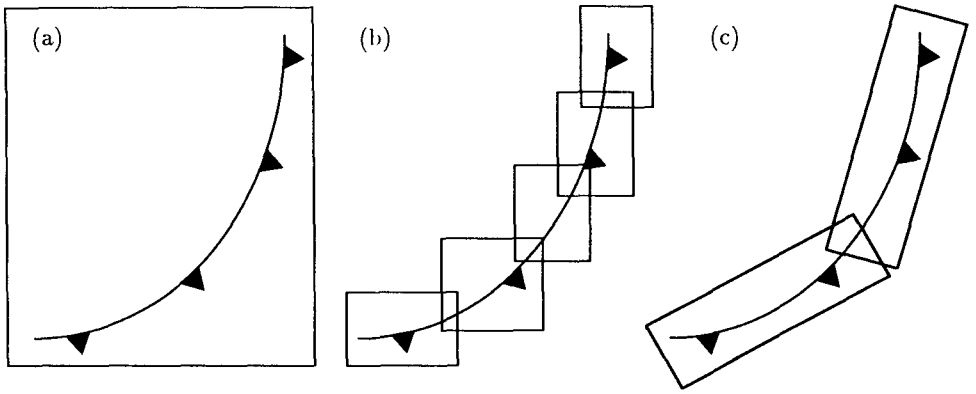

FIG. 1. Nested-grid example for (a) a single fine grid, (b) multiple, nonrotated fine grids, and (c) multiple, rotated fine grids. Multiple, rotated fine grids allow possible alignment with the flow and more economical coverage of the phenomena.

and a coarse grid length is an integer multiple of fine grid lengths. In this example we are considering the 2D problem; in three dimensions lengths are replaced by areas in (1).

Equation (1) can be satisfied during the updating process by appropriate averaging of the fine-grid values inserted onto the coarse grid; that is, $\Phi_I = \sum \phi_i \Delta l / \Delta L$. Interpolation formulas for boundary conditions can also be designed so that they satisfy (1). Kurihara et al. use a linear interpolation formula, and Clark and Farley use a quadratic formula, though it is formally only first-order accurate. All interpolation schemes that we are aware of are formally only first-order accurate.

Clark and Farley show that the use of conservative updating and interpolation schemes leads to superior solutions in their nested system. This has also been observed in applications of AMR in other fluid-flow problems such as transonic airflow (Berger and Jameson 1985) and incompressible Navier–Stokes calculations (Caruso et al. 1986; Perng 1990). These results can be expected in any system where there is a strict mass-conservation condition, such as in the anelastic equation set or incompressible Navier–Stokes equations, or in systems where small errors in the mass divergence can lead to large errors in the solutions, such as in systems containing shocks. Unfortunately, simple conservative interpolation and averaging formulas are not available for grids that are not aligned. Berger (1987) describes possible algorithms but they are complex. The remapping routines used in the arbitrary Lagrangian–Eulerian schemes (Dukowicz and Kodis 1987) are conservative but are complex and prohibitively expensive.

Hydrostatic nested and adaptive models generally have not used conservative interpolation and averaging procedures (for example, Skamarock et al. 1989; Zhang et al. 1986; Jones 1977; Harrison 1973; and others). The elastic nonhydrostatic system is similar to the hydrostatic system in that both have prognostic, hyperbolic equations for pressure, as opposed to the anelastic system and other systems that have diagnostic, elliptic equations for pressure. The similarity suggests that strictly conservative interpolation and averaging procedures are not essential for the elastic model. This has been found to be true for the elastic system, and further comment on this can be found in section 4. Since (1) does not need to be satisfied identically, general interpolation and averaging formulas can be applied, and grids do not need to be aligned.

3. 2D equations and discretization

For boundary conditions and updating tests, a simplified model is employed that utilizes the 2D, Boussinesq, dry-adiabatic equation set. The discretization follows Klemp and Wilhelmson (1978) with two significant modifications.

a. Equations and discretization

The inviscid, dry, adiabatic equations used in the 2D model are

$$\frac{\partial u}{\partial t} + \frac{\partial \pi}{\partial x} = -u\frac{\partial u}{\partial x} - w\frac{\partial u}{\partial z} \tag{2}$$

$$\frac{\partial w}{\partial t} + \frac{\partial \pi}{\partial z} - g\left(\frac{\theta}{\bar{\theta}} - 1\right) = -u\frac{\partial w}{\partial x} - w\frac{\partial w}{\partial z} \tag{3}$$

$$\frac{\partial \pi}{\partial t} + c_s^2\left(\frac{\partial u}{\partial x} + \frac{\partial w}{\partial z}\right) = 0 \tag{4}$$

and

$$\frac{\partial \theta}{\partial t} + w\frac{\partial \bar{\theta}}{\partial z} = -u\frac{\partial \theta}{\partial x} - w\frac{\partial(\theta - \bar{\theta})}{\partial z}. \tag{5}$$

Equations (2)–(5) are the horizontal and vertical momentum, pressure, and thermodynamic equations, respectively. The fluid velocities in x and z are u and

w, respectively; θ is the potential temperature; $\bar{\theta}(z)$ is the mean potential temperature, π is the perturbation Exner function [Exner function $\Pi = \bar{\Pi} + \pi = C_p\theta(p/p_0)^{R/C_p}$]; g is the gravitational constant; t is time; and c_s is the speed of sound. The sound speed is constant. This system is appropriate for shallow convection (Ogura and Phillips 1962) and is a Boussinesq system, except that compressibility has been retained for computational convenience. Alternatively, rescaling the velocities with a reference density would result in a system identical in form but appropriate for deep convection.

A time-split scheme is used whereby the terms responsible for the sound waves are separated from the remaining terms and integrated with a smaller time step. The discretization is similar to that developed by Klemp and Wilhelmson (1978). Differencing of the equations occurs on a staggered grid where the velocities u_i are defined at points a distance $\Delta x_i/2$ in the ith coordinate direction from the points where the pressure and potential temperature are defined (i.e., a C grid). The leapfrog time discretization requires integrating the equations from $t - \Delta t$ to $t + \Delta t$ with the time-tendency terms evaluated at time t. In this time-split scheme, terms responsible for both the acoustic and gravity wave modes [the left-hand side terms in (2) through (4)] are integrated from $t - \Delta t$ to $t + \Delta t$ with n small time steps of $\Delta\tau = 2\Delta t/n$. The advection terms are evaluated at time t and are held fixed over the small time steps. The new scheme presented here differs from that in Klemp and Wilhelmson in that the thermodynamic equation (5) is advanced with the small time step $\Delta\tau$ and the buoyancy term in (3) is evaluated on the small time step.

Defining averaging and differencing operators

$$\bar{\phi}^{\xi} = \frac{1}{2}(\phi_{\xi+\Delta\xi/2} + \phi_{\xi-\Delta\xi/2})$$

and

$$\delta_{\xi}\phi = \frac{1}{\Delta\xi}(\phi_{\xi+\Delta\xi/2} - \phi_{\xi-\Delta\xi/2}),$$

the discretizations for (2)–(5) are

$$\frac{u^{\tau+\Delta\tau} - u^{\tau}}{\Delta\tau} + \delta_x\pi^{\tau} - \alpha D_x = F_u \tag{6}$$

$$\frac{w^{\tau+\Delta\tau} - w^{\tau}}{\Delta\tau} + \frac{1}{2}(\delta_z\pi^{\tau} + \delta_z\pi^{\tau+\Delta\tau}) - \frac{g}{\bar{\theta}}\left[\frac{1}{2}(\overline{\theta^{\tau}}^{z} + \overline{\theta^{\tau+\Delta\tau}}^{z}) - \bar{\theta}\right] - \alpha D_z = F_w \tag{7}$$

$$\frac{\pi^{\tau+\Delta\tau} - \pi^{\tau}}{\Delta\tau} + c_s^2\delta_x u^{\tau+\Delta\tau} + \frac{c_s^2}{2}(\delta_z w^{\tau} + \delta_z w^{\tau+\Delta\tau}) = 0 \tag{8}$$

$$\frac{\theta^{\tau+\Delta\tau} - \theta^{\tau}}{\Delta\tau} + \frac{1}{2}(\overline{w^{\tau}\delta_z\bar{\theta}}^{z} + \overline{w^{\tau+\Delta\tau}\delta_z\bar{\theta}}^{z}) = F_{\theta}, \tag{9}$$

where

$$F_u = -\overline{\bar{u}^x\delta_x u}^x - \overline{\bar{w}^x\delta_z u}^z$$

$$F_w = -\overline{\bar{u}^z\delta_x w}^x - \overline{\bar{w}^z\delta_z w}^z$$

$$F_{\theta} = -\overline{[w\delta_z(\theta - \bar{\theta})]}^z - \overline{u\delta_x\theta}^x$$

and

$$D = \delta_x u^{\tau} + \delta_z w^{\tau}.$$

The terms on the right-hand sides of (6)–(9) are evaluated at time t. Equations (7), (8), and (9) are linear in z, and the vertical velocity w, the pressure π, and the potential temperature θ are obtained each small time step by inverting a single tridiagonal matrix for each column.

The method described above is stable, but some filtering is necessary to control noise when sharp fronts form. A second-order spatial filtering term is added to the rhs side of the momentum equations and the thermodynamic equation. The term is of the form $\nu\nabla^2$ and the values from time $t - \Delta t$ are used to maintain stability. Also, a time filter is needed to keep the different time levels of the solution coupled. The filter used is described by Robert (1966) and is

$$\phi^t = \tilde{\phi}_*^t + \gamma(\phi^{t-\Delta t} - 2\tilde{\phi}_*^t + \tilde{\phi}_*^{t+\Delta t}),$$

where the variables ϕ_* have yet to be filtered.

The primary differences between this discretization and the Klemp–Wilhelmson discretization is the introduction in the present scheme of the calculation of the buoyancy terms on the small time step, given in (7) and (9), and the addition of the terms involving the divergence in (6) and (7). A complete stability analysis for this system along with justification for the changes to the original KW scheme can be found in Skamarock and Klemp (1992).

Briefly, the additional terms in the momentum equation (αD_x, αD_z) act to damp the divergence and thus filter out the sound waves. Divergence damping has only negligible effect on other, nondivergent, modes in the system. The divergence used in the filter is the full divergence and not just the divergence of the horizontal velocity components. With the introduction of divergence damping, the offcentering of the vertically implicit piece of the small time step (see Durran and Klemp 1983) has been removed, and the time filtering has been decreased.

In the original KW model, where all the buoyancy calculations are performed on the large time step, the large time step is limited by the buoyancy frequency with the restriction being roughly of the form $N\Delta t < 1$. For small grids (Δx less than a few tens of kilometers), this stability restriction is not broached. However, with the application of nonhydrostatic models to larger-scale flows, larger Δt's are desired and this stability restriction becomes significant. By shifting the buoyancy calculations to the small time step, the max-

imum large time step is now limited only by the advection velocity and the dissipation terms.

b. *Boundary condition and updating algorithms*

For updating coarse-grid values that lie within a fine grid, the fine-grid values are first averaged over an equivalent coarse-grid volume, after which the new coarse-grid values are bilinearly interpolated from these averaged values. Interpolation is necessary when a fine grid is rotated with respect to a coarse grid because coarse- and fine-grid points may no longer coincide.

Boundary conditions are required for both the coarse and fine grids. The coarsest grid has its boundary conditions satisfied through some numerical representation of the physical boundary conditions. Fine-grid boundary conditions are obtained by quadratic spatial and linear temporal interpolation of all variables, except pressure, to the fine-grid boundaries from the interior of the coarser grid(s). The interpolated variables include a velocity normal to the boundary and, $\Delta x_n/2$ inward from the boundary, a tangential velocity and all other variables excluding pressure. Thus, the fine-grid boundary values vary linearly in time over both their large and small time steps. Note that this requires only a single interpolation of a coarse-grid tendency to the fine-grid boundary per coarse-grid time step; the tendency is held fixed over the fine-grid time steps.

As noted in section 2a, boundary values for overlapping fine grids must be interpolated from the other fine grid where possible. However, the fine grids are independently integrated over a single time step, and boundary values for the small time steps between t and $t + \Delta t$ are not yet available from the neighboring fine grid. In this case, the boundary values needed on the small time step between t and $t + \Delta t$ are linearly extrapolated using the boundary values at time t and $t - \Delta t$. The extrapolated values are replaced with the values interpolated from the overlapping fine grids after the full time step is complete for both grids. This procedure allows the grids to be independently integrated over the small time steps, with boundary values exchanged only at the end of the full time step.

The discretized pressure equation (8) needs no boundary conditions for solution on the interior grids; the finite-difference stencil is complete with the specification of the normal and tangential velocities. However, the boundary pressure calculations have been modified in two ways. A reduced sound speed is used when applying (8) to the pressure points at the boundaries (typically using $c_s = 100$ m s^{-1}), and after the small time steps and large time step are complete, the boundary pressures computed using the reduced sound speed are replaced with values interpolated from coarser grids or from an overlapping fine grid.

Two observations led to the use of these pressure boundary conditions. First, when the overlap between two fine grids is small, the use of (8) with no additional conditions on the pressure can produce a numerical instability. Decreasing the sound speed along the fine grid boundaries in the pressure equation (8) stabilizes the calculations for overlapped grids with very small overlaps. Second, if the boundary pressures computed using (8), with or without the reduced sound speed, are not replaced with values interpolated from the interior of another grid (either coarse or fine, computed using the correct sound speed), the pressure solution can diverge in a fine-grid overlap region or between the fine and coarse grid at the boundary.

We presently have no analysis that illuminates the nature of the overlap instability or shows why the modified pressure boundary conditions work. Intuitively, we surmise that using the reduced sound speed in computing the boundary pressure slows the sound waves, reduces reflection, and allows for more efficient removal of acoustic energy by filters in the model. By replacing the pressure at the end of the time step, the coarse- and fine-grid pressure fields remain closely coupled.

The linear temporal variation of the fine-grid boundary values does not allow for proper transmission of sound waves through boundaries. Proper acoustic transmission would require that boundary-value interpolations and updating occur every small time step. While the overhead associated with updating and interpolations is small in the present scheme, the overhead would not be insignificant if interpolations and updating occurred every small time step. For example, the cost of boundary interpolations and updating range from a few percent to 15%–20% of the total CPU time in the integrations presented in sections 4 and 5. The overhead depends on the complexity of the equation set and the size and distribution of fine grids. Also, the filtering of sound waves and the disregard for proper sound-wave transmission through the boundaries is consistent with the time-splitting approach; the sound waves have little energy and are meteorologically insignificant; hence, they are filtered and no effort is made to properly resolve them.

Other pressure boundary conditions have been tried. In particular, boundary pressure could be specified by interpolation as are all the other variables. This works well in the dry Boussinesq system but has led to some unstable calculations with the 3D, fully compressible moist model. As noted, the pressure can be allowed to float because (8) needs no boundary conditions in the C-grid discretization. In general, this produces noisy, poor solutions. Conservative interpolation and updating procedures can also be used with all of these conditions, but their use does not affect overall stability. Also, while the sound-wave filter discussed previously is sufficient to control sound-wave reflection at the boundaries when used with the conditions described previously, it does not stabilize other unstable conditions.

Yet another type of boundary condition is possible. The fine-grid boundary conditions described by Chen (1991) for use in a nested, nonhydrostatic split-explicit model are radiative with respect to sound waves. However, the boundary conditions described here are much simpler than those proposed by Chen. Divergence damping, and the adaptive philosophy of keeping phenomena that are poorly resolved on the coarse grid contained within the finer grids, appears sufficient for producing acceptable nested grid solutions.

Before continuing, we note that fine grids may overlap by varying amounts and there may be a considerable overlap in the case where the grids are rotated with respect to each other. When fine grids are not rotated, the grids can be positioned such that there are no points that are on the interior of both grids. In this case, the grids abut one another. Note that the overlap instability discussed in this section is most severe when grids abut. We consider boundary values to be part of the grid, and abutting grids are ones that have minimum overlap. In all adaptive solutions shown in this paper, the fine-grid boundary values are plotted along with the interior values, and grid boundaries are drawn on the outermost row of interpolated boundary values.

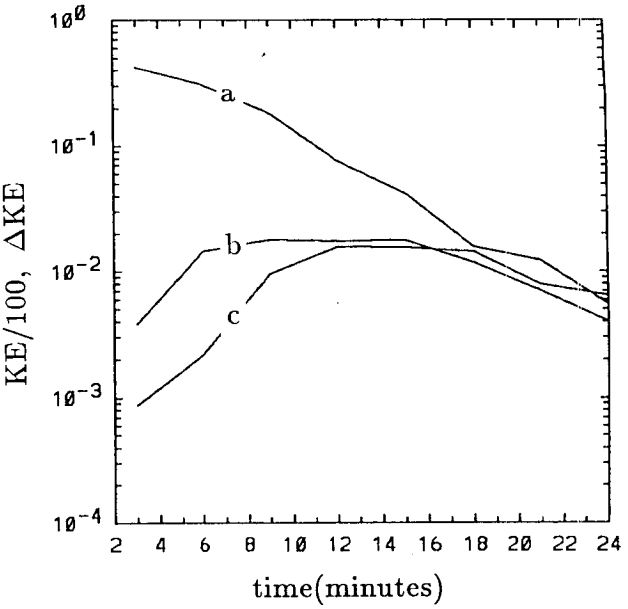

FIG. 2. (a) Total KE/100, (b) error kinetic energy from the Clark and Farley scheme, and (c) from the scheme described in section 3b for the bubble-collapse experiment.

4. 2D adaptive model examples

In this section, adaptive results for two different flows are presented. Both flows in the adaptive simulations result in horizontally propagating gravity currents, one starting from the release of a cold bubble in a closed box, and the other arising from the collapse of a cold pool (Skamarock and Klemp 1989). In the first simulation, the viscosity is fixed and a grid-independent solution is very nearly attained. However, in the second simulation the viscosity is a function of the resolution and the solution does not converge. This nonconvergence has implications for the evaluation of any solution computed with adaptive, nested, or any grid refinement models in which parameterizations are a function of the resolution.

Before discussing the gravity-current results, we note that the boundary and updating algorithms described in the previous section have also been tested by performing a series of collapsing bubble experiments similar to those performed by Clark and Farley (1984) and Orlanski (1976). The experiments are designed to test the propagation of gravity waves through the boundaries from fine to coarse grids and involve integrating a nested grid system using an initial condition consisting of a box of constant-θ air placed in an atmosphere of constant stability. In our test, a 9-km $\times$ 9-km domain and a 1.8-km square neutral bubble were used. Figure 2 depicts the error kinetic energy

$$\Delta\mathrm{KE} = \frac{\iint (\Delta u^2 + \Delta w^2)\, dA}{\iint dA}$$

along with the total kinetic energy for two nested bubble-collapse experiments, one using the Clark and Farley interpolation procedures and the other using those described in section 3b. Here Δu and Δw are the differences between velocities in the fine-grid solution and the nested solutions. The results of these experiments are similar to those presented in Clark and Farley but differ in one aspect. The conservative–reversible interpolation scheme does not improve the overall accuracy of the grid-nesting procedures for the elastic system.

a. Cold-bubble experiments

All physical boundaries in this simulation are solid, free-slip surfaces. The domain length is 24 km and its height is 12 km. The initial cold bubble is specified as follows:

$$\Delta\theta = \begin{cases} 0, & L \geq 1 \\ -15[\cos(\pi L) + 1]/2, & L < 1, \end{cases}$$

where

$$L = \left[\frac{(x - x_o)^2}{x_r^2} + \frac{(z - z_o)^2}{z_r^2}\right]^{1/2}$$

and $x_o = 0$, $x_r = 4000$ m, $z_o = 3000$ m, and $z_r = 2000$ m. The initial velocities are zero and the initial pressure π is computed by solving the anelastic pressure equation. The model parameters used in the runs are Δx_c, $\Delta z_c = 300$ m, $\Delta t_c = 4.0$ s, $\Delta\tau = 0.5$ s, $\alpha = 0.05$, and $\nu = 75$ m^2 s^{-1}.

Figures 3a and 3b depict the results at 900 s for fixed-grid simulations with 300- and 33.3-m resolution. The coarse-grid simulation cannot capture the billows that form behind the gust-front head. However, the general shape of the gravity current is well captured, and surprisingly, the gust-front position is the same in both the coarse- and fine-resolution simulations. Generally, the propagation of the gust front is independent of the resolution, though it does depend on the viscosity.

Adaptive simulation results are shown in Figs. 3c and 3d. In the adaptive simulations, the refinement ratio is 3 and the model computes the truncation errors and replaces the fine grids every 25 coarser-grid time steps. Thus, the fine grids are replaced every 100 s when one refinement level is used and, for two levels of refinement, the finest level grids are replaced every 33.3 s.

The adaptive simulation with a single level of refinement resolves the overall structure of the billows fairly well. There is still significant Gibbs phenomena associated with the propagating front and with the tail of the gravity current. The noise from the Gibbs phenomena is advected into the billows, particularly the leftmost billow. The adaptive simulation with two levels of refinement, where the finest grids have 33.3-m resolution, compares well with the single fine-grid run (compare Figs. 3b and 3d). The Gibbs phenomena are almost entirely removed and the position and shape of the billows are virtually identical in the two simulations. For most purposes, the solutions are identical, though there are small differences. For example, the middle billow in the fixed-grid simulation has a slightly colder core than that in the adaptive simulation.

The fine grids are not rotated in these simulations. We choose not to rotate the grids in order to always have gravity acting in a single coordinate direction. Fine-grid rotation in a 3D example will be demonstrated in the next section.

We have demonstrated that the adaptive method can produce results almost identical to fixed grid results having the same resolution as the finest grid in the adaptive simulations. For the adaptive method to be cost effective, that is, to actually justify its use, the CPU times and memory for the adaptive runs must be significantly less than that for the fixed grid runs. Table 1 presents the CPU times and approximate memory sizes for the adaptive- and fixed-grid codes. Obviously, increasing resolution increases both memory size and CPU times. Efficiency of the adaptive method is examined by comparing the 300–100-m adaptive run with the fixed 100-m-grid run and comparing the 300–100–33.3-m adaptive run with the fixed 33.3-m-grid run. With one level of refinement, the CPU time (from the fixed-grid run) and the required memory are both decreased by a factor of 3. Further refinement increases the efficiency. With two refinement levels, the CPU times are decreased by almost a factor of 7 and memory requirements are reduced similarly. The adaptive sim-

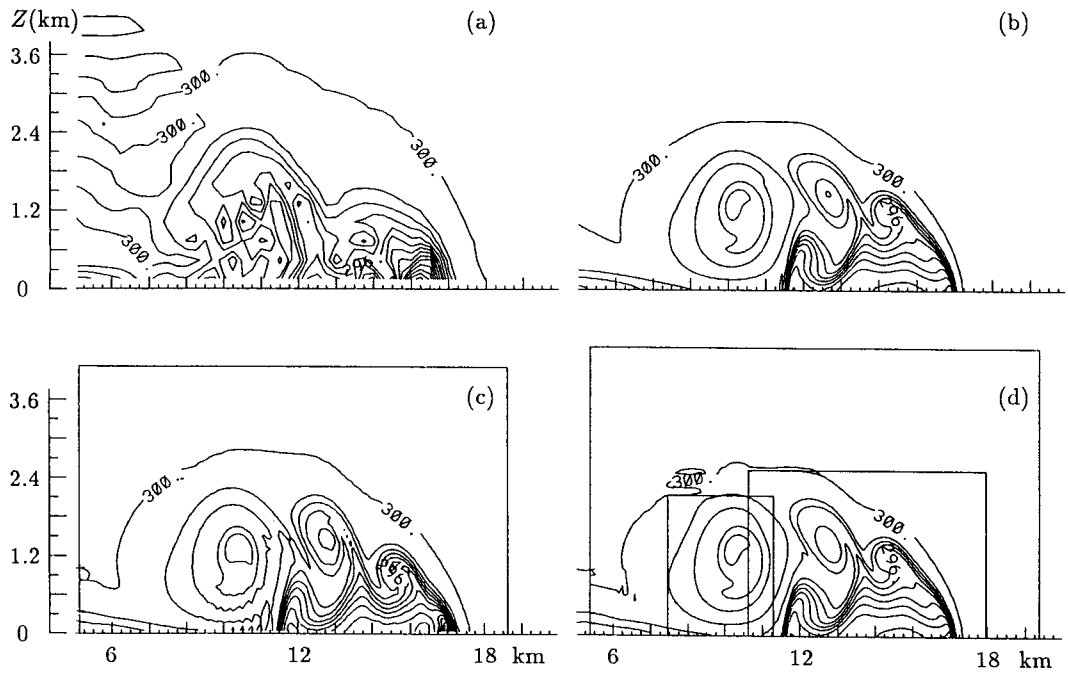

FIG. 3. Potential temperature fields for the cold-bubble simulation at 900 s with a contour interval of 1 for (a) a single grid with $\Delta x = \Delta z = 300$ m, (b) a single grid with $\Delta x = \Delta z = 33.3$ m, (c) an adaptive run with one level of refinement with $\Delta x_f = \Delta z_f = 100$ m, and (d) an adaptive run with two levels of refinement with $\Delta x_f = \Delta z_f = 33.3$ m. The contour interval is 1, and the fine grids in (c) and (d) are outlined.

TABLE 1. Program instructions and miscellaneous memory are an additional 700×10^3 words. All computations are performed on the NCAR CRAY Y-MP/864. The run times are with all plotting turned off.

Resolution (m)	CPU time (s)	Memory (thousands of words)
300	5.1	~60
100	94.3	~540
33	2288	~5000
300–100	35.3	~200
300–100–33	337.2	~1000

ulations are cost effective, and these results are consistent with those found in other applications of the AMR method.

Again it is emphasized that the AMR method is a *local* refinement method. The efficiency of the technique decreases as more area needs refinement. The break-even point for the method where the cost of an adaptive simulation will be approximately equivalent to a fixed-grid simulation occurs when about 50%–60% of the coarse domain needs refinement at the finest refinement level.

b. *Simulations of a collapsing cold pool*

The 2D adaptive model has also been used for simulating a collapsing surface cold pool and resulting gravity current, and the results are given in Skamarock and Klemp (1989). In these simulations, the upper, lower, and left boundaries are solid, free-slip surfaces, and the right boundary is open with boundary conditions specified as in Klemp and Wilhelmson (1978). The channel length is 40 km and the channel height is 10 km. The initial cold pool is specified as follows:

$$\theta = \begin{cases} 300 - \left(\dfrac{5000 - z}{5000}\, 10\right), & z \leqslant 5000 \text{ m}, \\ & x \leqslant 15\,000 \text{ m}; \\ 300, & \text{elsewhere.} \end{cases}$$

The initial velocities are zero and the initial pressure π is in hydrostatic balance with the temperature field. The model parameters used in the runs are $\Delta x_c = 250$ m, $\Delta t_c = 3.0$ s, $\Delta\tau = 0.5$ s, and $\nu = 0.012\Delta x^2/\Delta t$. In these simulations, the viscosity is now a function of the grid scale. The viscosity is chosen so that only well-resolved features are present on any grid. Decreasing the viscosity results in unacceptable noise in the solutions.

Figure 4 shows the solution for the collapsing cold pool at 900 s for two fixed-grid simulations. Figure 4a is the result from the coarse-grid run, and no billows are present behind the head of the gravity current because the viscosity mixes out any incipient billows. Several billows are present when the a 27.8-m grid is used (Fig. 4b). The presence of the billows in the fine-grid simulation is due entirely to the decreased mixing.

Results from an adaptive run with two levels of refinement (250-, 83.3-, and 27.8-m grids) are shown in Fig. 5. Comparing the fixed and adaptive grid runs with 27.8-m resolution (Figs. 4b and 5c) reveals a close correspondence. However, differences in certain solution features are apparent. In particular, the leftmost eddy that appears in the adaptive solution depicted in Fig. 5c does not appear in the reference solution in Fig. 4b. Examination of the evolving adaptive solution shows that perturbations associated with changing resolutions were sufficient to initiate the leftmost billow. The billow has sufficient truncation error associated with it to cause refinements to follow it.

Even changes in the numerical scheme can produce perturbations that excite the billow. Evidence for this is provided by the simulations presented in Carpenter et al. (1990), where a different numerical technique has been used to simulate the same problem. The leftmost eddy appears in their fine-resolution simulation and yet does not appear in their coarse-resolution results. However, changes to our boundary interpolations

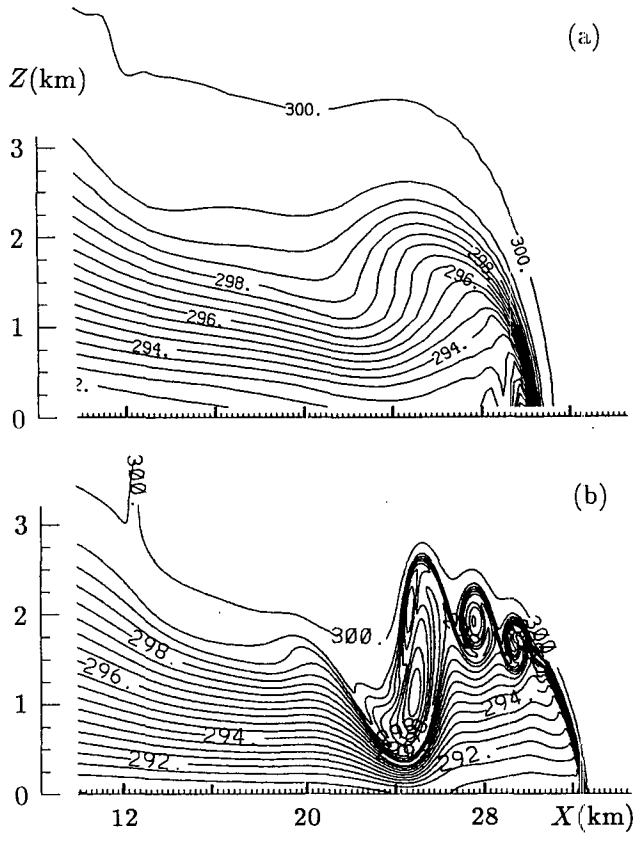

FIG. 4. Collapsing cold-pool simulation results at 900 s with potential temperature contoured at 0.5. (a) Single-grid solution with $\Delta x = \Delta z = 250$ m and (b) single-grid solution with $\Delta x = \Delta z = 28.7$ m.

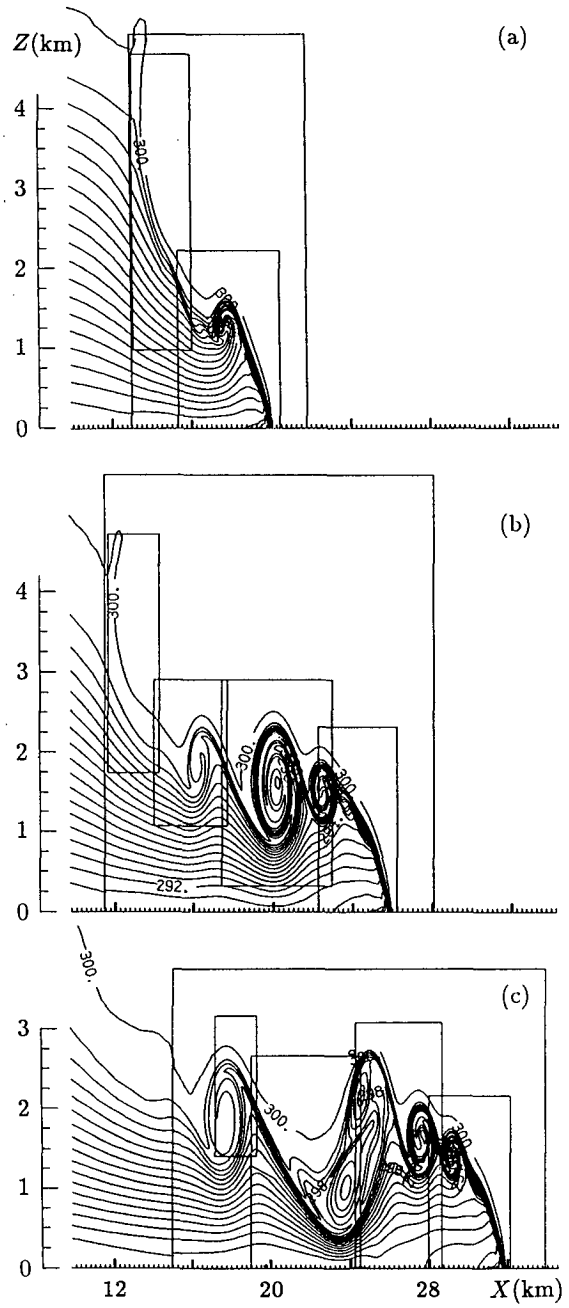

FIG. 5. Adaptive simulation results for the collapsing cold pool (a) at 300 s, (b) 600 s and (c) 900 s. Two refinement levels are used, $\Delta x_f = \Delta z_f = 28.7$ m, and the fine grids are shown. Contoured as in Fig. 4.

do not remove the fictious eddy. In particular, the use of conservative interpolations does not remove the eddy in this simulation.

The adaptive simulation depicted in Figs. 5a–c shows that the finer grids are replaced periodically as the solution evolves. The adaptive solution at 300 and 600 s is included to depict the changing grid structure over time. The finest level of grids is replaced 27 times over the course of this simulation. The solutions in the fine-grid overlap regions behave properly, and the procedure of obtaining boundary values from the overlapping grid correctly resolves finescale features passing through overlap regions.

c. *Convergence of solutions with parameterized physics*

The collapsing cold-pool simulations illustrate the difficulty in interpreting any simulations, particularly nested and adaptive simulations, when primary phenomena can arise from instabilities that grow from infinitesimal perturbations—as is the case with Kelvin–Helmholtz billows. Solutions will diverge as small perturbations are magnified. While this is primarily an issue of predictability rather than numerics, the use of physical parameterizations that depend on the grid scale exacerbate the predictability problem. In atmospheric models, it is usually necessary to parameterize processes that are not grid-resolvable—for example, turbulence, cloud microphysics, surface layers, etc. These parameterizations are dependent on the grid scale (Δx, Δt), and their effects change with varying grid scale. Questions of uniqueness thus arise when solving a system that contains parameterized physics. As Δx, $\Delta t \rightarrow 0$, do the finite-difference equations (parameterizations included) converge to a set of continuous equations that are well-posed and have a unique solution? In computational practice, we must ask if the solutions converge toward the solution of the continuous equations over the range in which Δx and Δt are altered.

The gravity-current results presented here lead us to these questions, as does the observation that the truncation error in simulations with parameterized mixing does not exhibit the expected rate of decrease with increasing resolution based on the usual truncation-error analysis for finer nested or adaptive grids, at times it even increases. Finer-scale structure appears on the fine grids that engender increased truncation error. This is not the case in models without parameterized physics.

The adaptive models seek to minimize the solution error by adaptively reducing the truncation error in regions where it is high. Given that the truncation error does not decrease and sometimes actually increases when using parameterizations that depend on grid scale, what can be said about the accuracy of the grid-refined solution? Without an exact solution, the concept of solution error no longer has precise meaning and can only be based on subjective criteria. There is no longer a single, definable solution error with which to directly connect the truncation error. Pragmatically, we must consider which refinement criteria will lead to the "best" solutions. Innumerable possibilities exist, and it is likely that additional refinement criteria should be included along with the truncation error. Certain

areas of the solution domain and certain flow features may be of more interest than others, and more subjective criteria for grid placement can be used to resolve these selected features.

A more fundamental concern is the validity and consistency of grid-scale-dependent parameterizations that are used over a wide range of grid scales, particularly in nested-grid and adaptive calculations. For example, it is known that convective parameterizations used in hydrostatic models will produce different convective realizations (time, location, and extent) solely due to a change in grid scale (Zhang and Fritsch 1988). It is also unclear at what grid scale the convective parameterizations become unnecessary and even detrimental. These same concerns apply to turbulence models and other parameterizations. In nested and adaptive models, grid-scale-dependent parameterizations must be carefully examined because we are demanding that they function over a wide range of grid scales and because they may have a substantial impact in an evolving adaptive solution.

The 2D examples illustrate the utility of the adaptive approach. We emphasize that the structure of the equations and the particular solution technique are what make possible these adaptive computations. The boundary approximation makes the computations economically attractive because boundary values do not need to be interpolated to interior boundaries on the small time step but rather only on the large time step. For elliptic equations and overlapping grids, the solution process described in this paper may not work because an elliptic equation represents a boundary-value problem, and the solution at any point depends upon all the boundary values. Iterative schemes known to give the correct solution for the overlapping grid problem are not economical.

Finally, we note that adaptive code is easily modified for applications in domain decomposition and parallel or distributed processing. The simplest approach consists of dividing the computational domain into regions (grids) of equal size and allowing each processor to work on a single grid. The overlapping boundary conditions, described in section 3d, are such that the solutions on overlapping grids do not exactly match the solution on the single, large grid because the small time-step boundary conditions do not allow sound waves to pass correctly through the boundaries. However, the differences in the solutions are insignificant, and the domain-decomposition model proves reasonably efficient when used on a multiprocessor CRAY.

5. 3D interactive model

A variation of the 3D Klemp–Wilhelmson model has been modified for use with the adaptive grid method. At this time, the model is not fully adaptive. Grid fitting in three dimensions is significantly more difficult than in two dimensions, and the 2D routines have not been extended to three dimensions. The more complex finite differencing in the 3D model also makes it more difficult to estimate truncation error. The model contains discretizations of different-order accuracy, and the procedure advocated by Berger and Oliger (1984) cannot be directly applied, nor is it easy to directly compute estimates of the truncation error using finite differencing.

Aside from grid-fitting and error-estimation routines, the 3D model possesses all the capabilities of the 2D adaptive model. In particular, multiple, overlapping, rotated fine grids are employed, and any number of fine grids and refinement levels can be used. The model is used interactively, and the user needs to specify the number, sizes, and locations of the fine grids. For example, in the convective simulations presented, the system was integrated in 10-min segments between which the fields were examined and the fine grids replaced. In these cases of strong convection, the fine grids are placed based on the locations of the updrafts, downdrafts, vorticity fields, and gust-front locations.

a. Model description

The 3D model used by the adaptive grid algorithms is an extension of the 2D model described in Miller and Durran (1991). The model includes terrain and moist processes (vapor, cloud, and rain water) and is fully compressible. The momentum equations and scalar equations for water substances are cast in flux form, and pressure is used as a prognostic variable. Moist physics are included through a Kessler parameterization scheme, calculated with the two-step procedure given by Soong and Ogura (1973). In the first step, the potential temperature and moisture are updated with the moist processes ignored. Next, the source and sink terms for potential temperature and moisture are calculated using the results from the first step. The second step ensures that total moisture and energy are conserved within the limits of the approximations and that both evaporation and condensation occur moist adiabatically.

The general time-stepping scheme has been altered to include the divergence damping terms. Also, the buoyancy term in the vertical momentum equation and the vertical advection of θ are now computed on the small time step. These changes are easily implemented.

b. Supercell storm simulations

The robustness of the nested-grid system used with the three-dimensional model is demonstrated in simulations of the 20 May 1977 Del City supercell storm. The convective event has been analyzed by Ray et al. (1981), Brandes (1981), and Klemp et al. (1981). Detailed analyses and simulations of its tornadic phase can be found in Klemp and Rotunno (1983, hereafter

referred to as KR) and Rotunno and Klemp (1985). Klemp et al. (1981) present simulations on a 48-km × 48-km horizontal domain with 1-km horizontal resolution and 500-m vertical resolution in a 16-km-depth domain. Klemp and Rotunno (1983) perform a *windowed* simulation wherein a fine grid with 250-m horizontal resolution is placed over the occlusion region of the supercell. The fine grid is initialized with interpolated coarse-grid values, but the grids are not integrated in the two-way interactive manner. Short time integrations on the fine grid are stable, and finescale structure in the occlusion region is revealed.

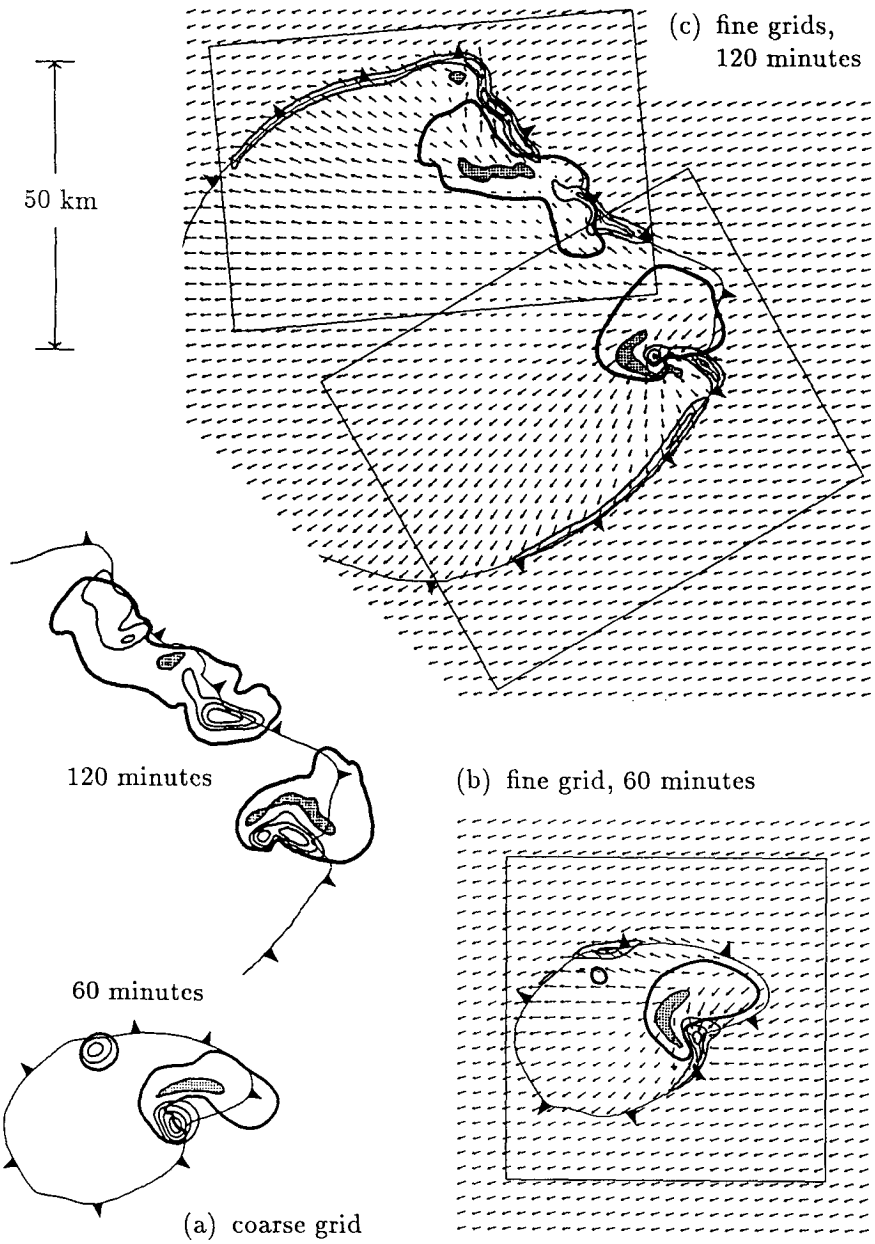

FIG. 6. Adaptive simulation of 20 May Del City supercell storm with $\Delta x_c = 3$ km, $\Delta x_f = 1$ km: (a) at $z = 3150$ m on the stationary coarse grid at 60 and 120 min, (b) at $z = 250$ m on the fine grid at 60 min, and (c) on the two fine grids at 120 min. The cold-frontal boundary in all figures is at $z = 250$ m and denotes the -1°C potential temperature perturbation. The heavy solid lines represent the 0.5 g kg^{-1} rainwater contour. Velocity vectors are for storm relative winds with storm velocities $U_s = 3$ m s^{-1} and $V_s = 14.6$ m s^{-1}. Vertical velocity is contoured at 1 m s^{-1} in (b) and (c) and at 5 m s^{-1} in (a) with the negative regions being stippled and zero contours removed.

We present two interactive simulations of the Del City storm. In the first, the coarse grid covers a 210-km × 210-km domain and has 3-km horizontal resolution. Fine grids in this simulation have a horizontal resolution of 1 km, and the vertical resolution of the coarse grid is 500 m. Figure 6 depicts the low-level flow field at 1 and 2 h. It also shows the fine-grid positions relative to the coarse grid and depicts the storm motion.

This simulation differs from Klemp et al. and most convective-storm simulations in that the coarse grid is stationary as opposed to the coarse grid moving at the average storm velocity, which in this case was approximately 15 m s^{-1} toward the east-northeast. Previously, computational limitations necessitated a moving domain that requires a priori knowledge of storm motion. In an adaptive or interactive simulation, a priori knowledge of storm motion is not needed as long as a sufficiently large coarse domain is used.

In addition to knowing storm motion, it has also been necessary to know the size of the evolving convective system. The 20 May storm splits early in its evolution; the right-moving storm is the supercell and the left-moving storm is much weaker. In the Klemp et al. simulations, the left-moving storm is allowed to propagate out of the domain because it has little bearing in their study and because it would be expensive to include both the right- and left-moving storms in a single computation. The interactive simulation shown in Fig. 6 captures both. Single and multiple overlapping fine grids are used to resolve both storms during the simulation.

The flow field near the surface at 60 min, shown in Fig. 6b, should be compared with KR Fig. 4b. The flow fields are similar; updrafts and downdrafts have the same relative magnitudes and shapes, the rainwater patterns are similar, and the gust fronts occupy the same position relative to the main updraft of the supercell.

Figure 6a in KR depicts the flow field at 120 min for the 1-km grid and can be compared with the lower-right fine grid at 120 min in Fig. 6c. The occlusion process in the adaptive model progresses more rapidly than in the KR simulation for the 1-km grid. We believe this is due primarily to the different mixing formulations in the two models; the KW model solves a prognostic turbulent kinetic energy equation, whereas TKE is diagnosed in the adaptive model (see Durran and Klemp 1983).

The vorticity field in the adaptive run at 120 min is given in Fig. 7. The strong cyclonic vorticity is similar in magnitude and location to that in KR. However, the strong anticyclonic vorticity present at the eastern edge of the occlusion on the 1-km fine grid is not apparent in KR Fig. 7b, neither does it appear on the KR 250-m grid (see KR Fig. 7d). This negative vorticity depicted at 120 min develops much earlier, beginning around 60 min, and alternately waxes and wanes until it strengthens dramatically when the occlusion process begins in earnest at approximately 90–100 min. This does not occur in the KR simulations until after 120 min.

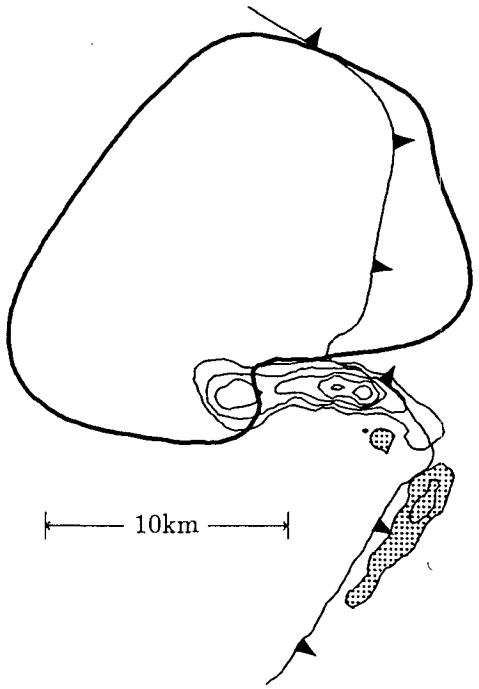

FIG. 7. Vorticity at 120 min with a contour interval of 0.005 s^{-1} for the field depicted in the lower right fine grid at 120 min. Negative vorticity is stippled.

Fine grids are replaced every 10 min in the simulations, and after 80 min, two fine grids are needed to track the right- and left-moving storms. The fine grids are placed so that features that would not be well resolved on the coarse grid are contained within a fine grid. The left-moving storm does not mature into a supercell, rather it develops a multicellular structure. If left unrefined on the 3-km grid, the left mover weakens dramatically. The right-moving supercell will not evolve into a strong supercell on the 3-km grid if left unrefined.

The solutions at the fine-grid boundaries are of particular numerical interest in the adaptive simulations. For the adaptive solution at 120 min (Fig. 6c), the solution in the fine-grid overlap region is smooth at both fine-grid boundaries. A strong updraft is propagating smoothly through one of the boundaries. The grids are not aligned with respect to each other, but given that the resolution is the same, simple interpolations do not introduce any significant error and the solutions stay well behaved. No extra filtering is performed at the boundaries. Also at 120 min, gust fronts are propagating out of both fine grids onto the coarse grid. The gust fronts do not pass smoothly through the boundary because they are poorly resolved on the coarse grid. The gust-front updraft appears to be par-

tially pinched off at the boundary, and the sharp temperature gradients associated with the gust front broaden as they pass to the coarse grid (not shown). The gust fronts were not followed any farther because, at this distance from the primary storm updrafts, inadequate resolution of the gust fronts has little effect on storm evolution.

In the second interactive simulation, a 1-km resolution coarse grid and 333-m fine grids are used to produce a simulation similar to that presented in KR. The KR 250-m grid simulation was started from a 1-km grid supercell at 120 min, a time when the low-level rotation had reached its maximum strength. The occlusion is not resolved on the 1-km grid of Klemp and Rotunno but is generated rapidly when the 250-m grid is used. Questions arise as to what effect the sudden increase in resolution has on the realism of the rapid occlusion that occurs after a sudden change in resolution. Occlusions have been observed to progress rapidly, and KR suggest two possible interpretations for their simulations. The first is that the finescale structures are forming on the coarser grid, though smoothed by the parameterized turbulence. The second suggestion is that the fine-grid simulation starts with the best estimate of the mature supercell structure and that the coarse grid does not capture any appreciable part of the occlusion dynamics. A simulation where fine resolution of the supercell is introduced well before the occlusion process will help resolve these questions. In the present interactive simulation, fine grids are used to resolve the developing supercell storm beginning after 0.5 h of simulated time. At 0.5 h, the initial updraft, triggered by the initial warm bubble, is well resolved and the precipitation downdraft is beginning to split the low-level updraft.

The low-level field for the 333-m grid is given in Fig. 8 at 60 min. Compared with the 1-km grid solution in KR Fig. 4b, the general features are similar and, as might be expected, the main updraft and gust fronts are narrower and slightly more intense on the 333-m grid. The most interesting new feature in the adaptive simulation are the waves present on the gust front extending to the southwest of the main supercell updraft. At this time, the waves are small amplitude and would not be resolved on a 1-km grid.

Figure 9 presents the low-level fields and vorticity at 80, 110, and 120 min. During this time period, the storm occludes and, as in the other adaptive simulation, the supercell evolves more rapidly in the adaptive simulations than in the KR simulation. The adaptive simulations at 120 min and the KR 250-m simulation share many flow features. In both simulations, the downdraft progresses cyclonically around the circulation center (see KR Fig. 7c). A ring of cyclonic vorticity is forming around the circulation center and, as in KR, the increasing low-level vorticity associated with storm occlusion is only slowly communicated to the upper levels. Two updraft maxima form: the original maxima

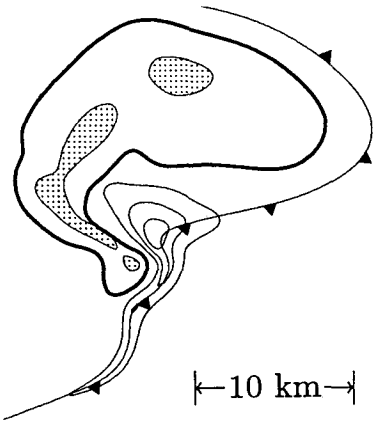

FIG. 8. Adaptive simulation of the 20 May 1977 Del City supercell storm with $\Delta x_c = 1$ km and $\Delta x_f = 333.3$ m. Fields at $z = 250$ m at 60 min for the fine grid. Plotting is as in Fig. 6.

is at the center of the occlusion and the second is at the northeastern edge of the occlusion in response to the strong convergence forced by the rapidly propagating gust front. The vorticity maxima in the 333-m solutions are two to three times larger in magnitude than those in the 1-km solutions, though they are not as strong as in the KR 250-m simulation. The strong anticyclonic vorticity to the south of the eastern tip of the occlusion is still present and it has the same magnitude as the maximum cyclonic vorticity.

The adaptive solution shows a wave propagating to the southwest along the gust front that is absent from the KR simulation. Point A in Figs. 9a–c denotes the position of a single wave over time. The wavelength increases as the wave propagates, and the wave is responsible for a positive and negative vorticity couplet. At 110 min (Fig. 9b), a second smaller wave is apparent immediately behind (to the north of) the larger wave. The positive and negative vertical vorticity couplet associated with the waves is a clear signal of their presence. These waves have been produced in high-resolution simulations with other cloud models (R. Wilhelmson, personal communication).

Simulations have been performed where refinement is introduced at later times and the results have been different. If high resolution is introduced late in the simulation, rapid occlusion occurs, much as when KR introduces the 250-m grid. The occlusion process, when refinement begins at an early time, is a more gradual process. However, comparison of the 1-km and 333-m solutions shows that the coarser grid does capture the larger-scale features well. This suggests that the KR results for the 250-m grid are reasonable, though the time evolution is probably somewhat accelerated; the 333-m results suggest that the major finescale features discussed here form over a 10–20-min time interval.

As in the previous adaptive simulations, the solution at the fine-grid boundaries is well behaved, and finescale

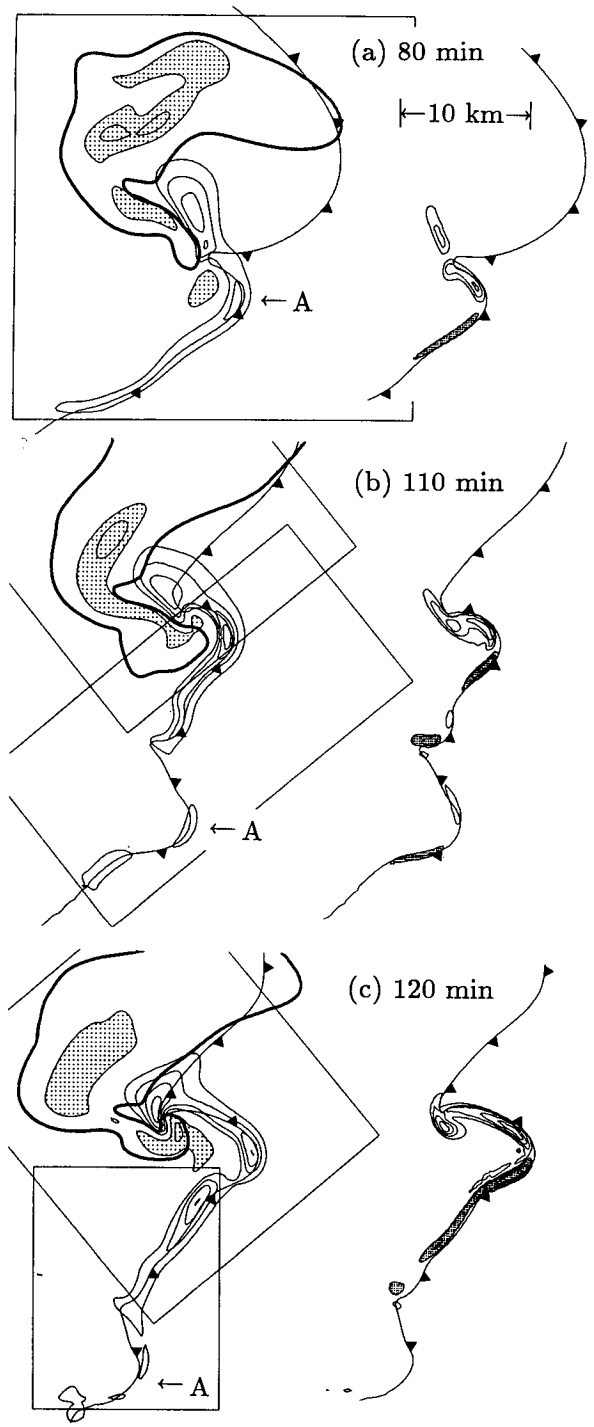

FIG. 9. Fields and vorticity at $z = 250$ m for the fine grids at (a) 80 min, (b) 110 min, and (c) 120 min. The vorticity is plotted to the right of the flow fields. Plotting is as in Figs. 7 and 8.

disturbances pass smoothly through boundaries of overlapping fine grids. Again, finescale features do not pass cleanly from the fine to the coarse grid in cases where the coarse grid cannot adequately resolve the features. The adaptive approach dictates that these features should be followed with refinements until they either propagate out of the physical domain or decay. In atmospheric calculations, however, it will not always be possible to refine all small-scale flow features.

Finally, single fine-grid calculations for the 3D model have not been performed because the computational resources were not available. The 3D model appears to be relatively more efficient than the 2D model based on the observation that the 3D model spends over 85% of its CPU time in the solver, compared with 75% of the CPU time used by the solver in the 2D model.

6. Summary

We have presented results from 2D and 3D adaptive grid models that solve nonhydrostatic, elastic equation sets. The simulations demonstrate the utility of the adaptive grid approach. In particular, for local phenomena, the adaptive method can be used to produce accurate solutions at only a fraction of the CPU and memory requirements of an equivalent fixed fine-grid solution. Presently, the 2D model is fully automated and the 3D model is used interactively.

The adaptive method makes use of regular nested refinements. This approach allows the use of regular, fast, preexisting solvers. Any number of refinements and refinement levels can be used, as opposed to the moving-gridpoint methods where the number of points is fixed. The use of rotated, overlapping refinements permits economical coverage of areas needing refinement. The multiple-grid solution technique also facilitates the use of simple domain decomposition and parallel processing.

Simple approaches to rendering the 3D model fully adaptive (automatic) are being investigated. In particular, the 2D grid-fitting routine can be used to fit grids in the two horizontal dimensions, with no refinement used in the vertical. Simple refinement criteria can be used, such as vorticity, gradients of the prognostic variables, etc., and vertically integrated measures of these refinement criteria can be passed to the existing 2D grid-fitting routines. In many cases—for example, that of strong convection—simple refinement criteria will bring about reasonable grid placement. In more complex situations, the question of appropriate refinement criteria will need to be addressed. For examining the role of convection embedded in larger-scale environments, vertical refinement is not critical because the large-scale typically has sufficient vertical resolution for resolving the active convection on nested grids that have horizontal resolutions of 1 km. In general, we believe that vertical refinement is not appropriate until the horizontal resolution is of the same order as the vertical resolution.

We have introduced several numerical procedures for use in the adaptively nested, nonhydrostatic, elastic, time-split model. Inner-grid boundary conditions are

slightly different than those in traditional nested models. Data transfers between coarse and fine grids take place only after large time steps, not after each small (acoustic) time step. For the inner fine grids, boundary values are interpolated linearly in time and quadratically in space from the coarse grid. The exception to this is for the pressure, which is computed at the boundaries using a reduced sound speed and replaced after the small time steps are complete. Grids with the same resolution that overlap must obtain their boundary values from the other overlapping grid. Both the 2D and 3D simulations demonstrate the robustness of these inner-grid boundary conditions for both fine and overlapping grids.

A divergence filter, as described in Skamarock and Klemp (1992), is used in these models. The inner-grid boundary conditions do not take into account acoustic waves, and this filter effectively removes them. We also integrate the equation for potential temperature differently than in past models; the vertical advection of the mean θ and the buoyancy term in the vertical momentum equation is updated on the small time step. This effectively removes any stability restrictions arising from gravity-wave propagation and removes instabilities related to buoyancy–sound-wave interaction.

Subgrid-scale parameterizations cannot necessarily be discarded when using AMR because they may be critical in the initiation of important phenomena, which, while being subgrid scale on a coarse grid, will be explicitly resolved on the fine grid. In the case of imminent convection, refinement criteria other than the truncation error may need to be used to bring about the necessary refinement in a timely manner in cases where the convection is not resolved on the coarse grid. This may also be the case for other phenomena. Also note that parameterizations that depend on the grid scale can be the cause of nonconvergent solutions in any adaptive or nested model. These parameterizations effects leave open the following questions. 1) What is the correct solution? 2) When using adaptive models, how far should refinement proceed?

Adaptive mesh refinement, with its ability to resolve isolated small-scale phenomena within larger-scale flows, makes possible the exploration of several scale-interaction problems. On present supercomputers, the adaptive models should permit maximum solution refinement of between one and two orders of magnitude. Using these computational capabilities, our continuing adaptive work focuses on the explicit resolution of convection in realistic larger-scale environments.

Acknowledgments. The first author was partially funded under NSF Grant ATM 8809862.

REFERENCES

Berger, M., 1987: On conservation at grid interfaces. *SIAM J. Num. Anal.*, **24,** 967–984.

——, and J. Oliger, 1984: Adaptive mesh refinement for hyperbolic partial differential equations. *J. Comput. Phys.*, **53,** 484–512.

——, and A. Jameson, 1985: Automatic adaptive grid refinement for the Euler equations. *AIAA J.*, **23,** 561–568.

——, and P. Colella, 1989: Local adaptive mesh refinement for shock hydrodynamics. *J. Comput. Phys.*, **82,** 64–84.

Brandes, E. A., 1981: Fine structure of the Del City–Edmond tornado mesocirculation. *Mon. Wea. Rev.*, **106,** 995–1011.

Carpenter, R. L., K. K. Droegemeier, P. R. Woodward, and C. E. Hane, 1990: Application of the piecewise parabolic method (PPM) to meteorological modeling. *Mon. Wea. Rev.*, **118,** 586–612.

Caruso, S. C., J. H. Ferziger, and J. Oliger, 1986: Adaptive grid techniques for elliptic flow problems. AIAA 24th Aerospace Sciences Meeting Paper AIAA-86-0498.

Clark, T. L., and R. D. Farley, 1984: Severe downslope windstorm calculations in two and three spatial dimensions using anelastic interactive grid nesting: A possible mechanism for gustiness. *J. Atmos. Sci.*, **41,** 329–350.

Chen, C., 1991: A nested grid, nonhydrostatic, elastic model using a terrain following coordinate transformation: The radiative-nesting boundary conditions. *Mon. Wea. Rev.*, **119,** 2852–2869.

Dannenhoffer, J. F., and J. R. Baron, 1986: Robust grid adaptation for complex transonic flows. AIAA 24th Aerospace Sciences Meeting Paper AIAA-86-0495.

Dietachmayer, G. S., 1992: On the application of continuous dynamic grid adaptation techniques to meteorological modeling. Part II: Efficiency. *Mon. Wea. Rev.*, **120,** 1707–1722.

——, and K. K. Droegemeier, 1992: On the application of continuous dynamic grid adaption techniques to meteorological modeling. Part I: Basic formulation and accuracy. *Mon. Wea. Rev.*, **120,** 1675–1706.

Dukowicz, J. K., and J. W. Kodis, 1987: Accurate conservative remapping (rezoning) for arbitrary Lagrangian-Eulerian computations. *SIAM J. Sci. Stat. Comput.*, **8,** 305–321.

Durran, D. R., and J. B. Klemp, 1983: A compressible model for the simulation of moist mountain waves. *J. Atmos. Sci.*, **111,** 2341–2361.

Harrison, E. J., 1973: Three-dimensional numerical simulations of tropical systems utilizing nested finite grids. *J. Atmos. Sci.*, **30,** 1528–1543.

Hawken, D. F., J. J. Gottlieb, and J. S. Hansen, 1991: Review of some adaptive node-movement techniques in finite-element and finite-difference solutions of partial differential equations. *J. Comput. Phys.*, **95,** 254–302.

Hoke, J. E., N. A. Phillips, G. J. DiMego, J. J. Tuccillo, and J. G. Sela, 1989: The regional analysis and forecast system of the National Meteorological Center. *Wea. Forecasting*, **4,** 323–334.

Jones, R. W., 1977: A nested grid for a three-dimensional model of a tropical cyclone. *J. Atmos. Sci.*, **34,** 1528–1553.

Kallinderis, Y. G., and J. R. Baron, 1989: Adaptation methods for a new Navier–Stokes algorithm. *AIAA J.*, **27,** 37–43.

Klemp, J. B., and R. B. Wilhelmson, 1978: The simulation of three-dimensional convective storm dynamics. *J. Atmos. Sci.*, **35,** 1070–1096.

——, and R. Rotunno, 1983: A study of the tornadic region within a supercell storm. *J. Atmos. Sci.*, **40,** 359–377.

——, R. B. Wilhelmson, and P. S. Ray, 1981: Observed and numerically simulated structure of a mature supercell thunderstorm. *J. Atmos. Sci.*, **38,** 1558–1580.

Kurihara, Y., G. J. Tripoli, and M. A. Bender, 1979: Design of a movable nested-mesh primitive equation model. *Mon. Wea. Rev.*, **107,** 239–249.

Miller, P. P., and D. R. Durran, 1991: On the sensitivity of downslope windstorms to the asymmetry of the mountain profile. *J. Atmos. Sci.*, **48,** 1457–1473.

Ogura, Y., and N. A. Phillips, 1962: Scale analysis of deep and shallow convection in the atmosphere. *J. Atmos. Sci.*, **19,** 173–179.

Oliger, J., W. C. Skamarock, and W. P. Tang, 1990: Convergence analysis and acceleration of the Schwarz alternating method. *Sci. Stat. Comp. J. Soc. Indust. Appl. Math.*

Orlanski, I., 1976: A simple boundary condition for unbounded hyperbolic flows. *J. Comput. Phys.*, **21,** 251.

Perng, C. Y., 1990: Adaptive-multigrid computations for incompressible flows, including geometry, temperature, and salinity effects. Ph.D. dissertation, Department of Mechanical Engineering, Stanford University.

Ray, P. S., B. C. Johnson, K. W. Johnson, J. S. Bradberry, J. J. Stephens, K. K. Wagner, R. B. Wilhelmson, and J. B. Klemp, 1981: The morphology of several tornadic storms on 20 May 1977. *J. Atmos. Sci.*, **38,** 1643–1663.

Robert, A. J., 1966: The integration of a low order spectral form of the primitive meteorological equations. *J. Meteor. Soc. Japan,* **44,** 237–245.

Rotunno, R., and J. B. Klemp, 1985: On the rotation and propagation of simulated super-cell thunderstorms. *J. Atmos. Sci.*, **42,** 271–292.

Skamarock, W. C., 1989: Truncation error estimates for refinement criteria in nested and adaptive models. *Mon. Wea. Rev.*, **117,** 882–886.

——, and J. B. Klemp, 1989: Adaptive models for 2-D and 3-D atmospheric flow. Preprints, *6th Int. Conf. on Numerical Methods in Laminar and Turbulent Flow,* Swansea, Wales, 1413–1424.

——, and ——, 1992: The stability of time-split numerical schemes for the hydrostatic and nonhydrostatic elastic equations. *Mon. Wea. Rev.*, **120,** 2109–2127.

——, J. Oliger, and R. L. Street, 1989: Adaptive grid refinement for numerical weather prediction. *J. Comput. Phys.*, **80,** 27–60.

Soong, S. T., and Y. Ogura, 1973: A comparison between axi-symmetric and slab-symmetric cumulus cloud models. *J. Atmos. Sci.*, **34,** 344–355.

Thompson, M. C., and J. F. Ferziger, 1989: An adaptive multigrid technique for the incompressible Navier-Stokes equations. *J. Comput. Phys.*, **82,** 94–121.

Zhang, D.-L., and J. M. Fritsch, 1988: Numerical sensitivity experiments of varying model physics on the structure, evolution and dynamics of two mesoscale convective systems. *J. Atmos. Sci.*, **45,** 261–293.

——, H.-R. Chang, N. L. Nelson, T. T. Warner, and J. M. Fritsch, 1986: A two-way interactive nesting procedure with variable terrain resolution. *Mon. Wea. Rev.*, **114,** 1330–1339.